

The OmegaWhite survey for short-period variable stars – VII. High amplitude short-period blue variables

Gavin Ramsay¹,^{1*} Patrick A. Woudt,² Thomas Kupfer,³ Jan van Roestel⁴,⁴ Kerry Paterson,^{2,5} Brian Warner,² David A. H. Buckley⁶,^{2,6} Paul J. Groot,^{2,6,7} Ulrich Heber,⁸ Andreas Irrgang,⁸ C. Simon Jeffery⁹,¹ Mokhine Motsoaledi,^{2,6} Martinus J. Schwartz² and Thomas Wevers^{1,9}

¹Armagh Observatory & Planetarium, College Hill, Armagh BT61 9DG, UK

²Department of Astronomy, Inter-University Institute for Data-Intensive Astronomy, University of Cape Town, Private Bag X3, Rondebosch 7701, South Africa

³Department of Physics and Astronomy, Texas Tech University, PO Box 41051, Lubbock, TX 79409, USA

⁴Division of Physics, Math, and Astronomy, California Institute of Technology, Pasadena, CA 91125, USA

⁵Center for Interdisciplinary Exploration and Research in Astrophysics & Dept Physics and Astronomy, Northwestern University, Evanston, IL 60208-3112, USA

⁶South African Astronomical Observatory, PO Box 9, Observatory 7935, South Africa

⁷Department of Astrophysics/IMAPP, Radboud University, PO Box 9010, NL-6500 GL Nijmegen, the Netherlands

⁸Dr Karl Remeis-Observatory & ECAP, Friedrich-Alexander University Erlangen-Nürnberg, Sternwartstr. 7, D-96049 Bamberg, Germany

⁹European Southern Observatory, Alonso de Córdova 3107, Vitacura, Santiago, Chile

Accepted 2022 April 6. Received 2022 April 6; in original form 2022 February 16

ABSTRACT

Blue Large-Amplitude Pulsators (BLAPs) are a relatively new class of blue variable stars showing periodic variations in their light curves with periods shorter than a few tens of minutes and amplitudes of more than 10 per cent. We report nine blue variable stars identified in the OmegaWhite survey conducted using ESO’s VST, which shows a periodic modulation in the range 7–37 min and an amplitude in the range 0.11–0.28 mag. We have obtained a series of followup photometric and spectroscopic observations made primarily using SALT and telescopes at SAAO. We find four stars which we identify as BLAPs, one of which was previously known. One star, OW J0820–3301, appears to be a member of the V361 Hya class of pulsating stars and is spatially close to an extended nebula. One further star, OW J1819–2729, has characteristics similar to the sdAV pulsators. In contrast, OW J0815–3421 is a binary star containing an sdB and a white dwarf with an orbital period of 73.7 min, making it only one of six white dwarf-sdB binaries with an orbital period shorter than 80 min. Finally, high cadence photometry of four of the candidate BLAPs show features that we compare with notch-like features seen in the much longer period Cepheid pulsators.

Key words: astronomical data bases: surveys – binaries – stars: oscillations – stars: variable.

1 INTRODUCTION

Over the last several decades, variable star research has been transformed by wide-field photometric surveys, such as the All-Sky Automated Survey for Supernovae (Shappee et al. 2014) and the Optical Gravitational Lensing Experiment (OGLE; Udalski, Szymański & Szymański 2015), to name just two. Although these surveys were particularly well-suited to identifying long-period variables such as Cepheid and RR Lyr stars, e.g. the Catalina survey which discovered thousands of new RR Lyr stars (Drake et al. 2013), populations of short-period variables (tens of minutes) have also been discovered.

One such short-period variable identified in OGLE data appears to be the prototype of a new class of variable star. OGLE-GD-DSCT-0058 was found to be periodic on a time-scale of 28.3 min and has a photometric amplitude of 0.24 mag in the *I* band (Pietrukowicz et al. 2015). They derived a temperature of 33 000 K from its spectrum indicating it was far too hot for it to be a δ Sct star. Pietrukowicz

et al. (2017) later found an additional 13 stars with similar properties and dubbed them ‘Blue Large-Amplitude Pulsators’ (BLAPs). They show light curves that are ‘saw-toothed’ and are similar in shape to that of RR Lyr or Cepheid pulsators.

Since then Kupfer et al. (2019, 2021) identified four and 12 short-period blue variable stars, respectively, using Zwicky Transient Factory (ZTF) data taken at high cadence and at low-Galactic latitude (Bellm et al. 2019; Graham et al. 2019). Although their temperature is similar to the BLAPs reported by Pietrukowicz et al. (2017), their periods (3.3–16.6 min) are shorter and amplitude (2–12 per cent) are lower. Kupfer et al. (2019) suggested that the new variables were lower-mass, higher-gravity analogues of the BLAPs and perhaps part of the same class of pulsators but at different stages of their evolution.

BLAPs are interesting in that it is difficult for stars to pulsate on such a short period with such a high amplitude. Romero et al. (2018) and Byrne & Jeffery (2018) have performed studies on their formation channels with the former proposing they are the hot counterparts of stars, which lead to the formation of extremely low mass (ELMs) white dwarfs and the latter testing whether post-common envelope stars could be their origin. Byrne & Jeffery (2020) subsequently demonstrated that pre-ELM white dwarf models, which

* E-mail: Gavin.Ramsay@armagh.ac.uk

include chemical diffusion, will switch on their pulsations precisely, where BLAPs are observed. In addition, Byrne & Jeffery (2020) also concluded that a channel where BLAPs were formed from binaries in which Roche lobe overflow was occurring merited further investigation. Byrne, Stanway & Eldridge (2021) explore possible reasons for why stars with gravities between the high-gravity and low-gravity BLAPs do not appear to pulsate despite models predicting they should.

Because of their short period, BLAPs are more likely to be identified in wide field surveys with high cadence – as was the case with the ZTF survey of the Galactic plane (Kupfer et al. 2019). Another well-suited survey is the OmegaWhite (OW) survey which was a high cadence survey of the southern Galactic plane and covered ~ 400 square degrees and was sensitive to time-scales as short as a few minutes (Macfarlane et al. 2015; Toma et al. 2016).

Although multiband colour information is available for many of the OW fields from the VPHAS+ survey (Drew et al. 2014), determining the nature of variable stars found in the OW survey is not trivial. However, with the release of the *Gaia* DR2/EDR3 catalogues, it is now possible to identify candidate BLAPs in a more robust manner. Ramsay (2018) cross-matched the BLAPs reported by Pietrukowicz et al. (2017) with *Gaia* DR2 and dereddened the colour and absolute magnitude to determine which part of the $BP - RP$, M_G colour–magnitude diagram BLAPs lie. Furthermore, McWhirter & Lam (2022) used *Gaia* DR2 and ZTF DR3 data to identify 22 candidate BLAPs.

In this paper, we search for stars which have photometric characteristics of BLAPs in the OW survey and have *Gaia* dereddened $BP - RP$, M_G colour magnitudes which are consistent with the known BLAPs. For stars which we identify as candidate BLAPs, we obtained followup photometry and spectroscopy mainly using Southern African Large Telescope (SALT) and telescopes at SAAO.

2 IDENTIFYING BLAPs IN THE OW SURVEY

The OW survey was conducted using the European Southern Observatory *VLT Survey Telescope* (*VST*), located at Paranal in Chile, with the OmegaCam 1 square degree camera between 2011 December and 2018 February and covered 404 square degrees. A series of 39 s images were taken in the g band of the same field for ~ 2 h and photometry was obtained using the difference imaging code DIAPL2 (Wozniak 2000), which is an adaptation of the original algorithm outlined in Alard & Lupton (1998). Full details of the reduction process can be found in (Macfarlane et al. 2015; Toma et al. 2016).

A key strand of the OW project is followup observations of sources identified using the *VST* data. The first set of followup data was presented by Macfarlane et al. (2017a), with more detailed observations of a rotating DQ white dwarf shown in Macfarlane et al. (2017b). Toma et al. (2016) noted one source, OW J1810385–2516086, which has a period of 28.9 min and an amplitude of 0.42 mag. Its colours ($g - r = 1.11$, $u - g = -0.50$) suggest an intrinsically blue source which is significantly reddened. Toma et al. (2016) also showed that the source OW J1811002–2730133 had a period of 23.1 min and an amplitude of 0.46 mag but did not have colour information at that time.

We made a systematic search for additional objects which show high amplitude short-period modulation in the OW survey. We restricted our search for sources brighter than $g \sim 19$; had a maximum peak in its Generalised Lomb-Scargle (LS) periodogram (Press et al. 1992; Zechmeister & Kürster 2009) less than 40 min with a false alarm probability (FAP) of $\log(\text{FAP}) < -2.5$; and modulation amplitude > 0.1 mag. All candidate variables which passed these

criteria were then passed through a manual verification process to determine that the period and amplitude were not due to instrumental artifacts. For instance, Toma et al. (2016) show that because of the alt-az nature of the *VST* mount, diffraction spikes from bright stars appear to rotate with respect to stars in the image and can cause sources which are near these bright stars to show a spurious period in their light curve.

We then cross-matched those stars which passed our selection and vetting process with the *Gaia* EDR3 catalogue (Gaia Collaboration 2021). We convert the parallax taken from *Gaia* EDR3 into distance following the guidelines from Bailer-Jones (2015), Astraatmadja & Bailer-Jones (2016) and Gaia Collaboration (2018), which is based on a Bayesian approach. In practise, we use a routine in the STILTS package (Taylor 2006) and apply a scale length $L = 1.35$ kpc, which is the most appropriate for stellar populations in the Milky Way in general. We use this distance to determine the absolute magnitude in the *Gaia* G band, M_G using the mean *Gaia* G magnitude. We then deredden the $(BP - RP)$; the blue and red magnitudes derived from prism data), M_G values using the 3D-dust maps derived from Pan-STARRS1 data (Green et al. 2018). For stars just off the edge of the Pan-STARRS1 field ($\delta < -30^\circ$), we took the nearest reddening distance relationship: further details of the procedure are outlined in more detail by Ramsay (2018). Given that the parallaxes are generally small (Table 1), the distances and hence M_G are rather uncertain. We selected those stars which have positions in the $(BP - RP)_o$, M_{G_o} plane which are bluer than stars in the main sequence but with $2 < M_{G_o} < 10$ (i.e. brighter than the white dwarf tracks and fainter than the BLAPs of Pietrukowicz et al. 2017).

There are nine stars which passed these stages and which we identified as candidate BLAPs. We show their sky co-ordinates, period, g mag, amplitude, $(BP - RP)$, M_G in Table 1. They have a range in period between 7.4 and 36.7 min, amplitudes between 0.11 and 0.42 mag, and $16.6 < g < 19.6$. We now present dedicated photometric and spectroscopic observations of these sources, which enables us to determine their nature.

3 HIGH SPEED PHOTOMETRY

We obtained followup photometry of five of the sources outlined in Table 1, using the SAAO 1.0m telescope and the Sutherland High-Speed Optical Cameras (SHOC; Coppejans et al. 2013) at Sutherland, South Africa. We indicate the time and duration of these photometric observations together with the exposure time and filter in Table 2.

The data were reduced using standard procedures in IRAF. Light curves were derived using aperture-corrected photometry, calibrated using Pan-STARRS g -band photometry (Chambers et al. 2016). We then used the VARTOOLS suite of software (Hartman et al. 2008) to obtain a power spectrum for each light curve using the LS implementation. We show the period, amplitude, and FAP of the peak in the power spectra in Table 2.

4 FOLLOWUP SPECTROSCOPIC OBSERVATIONS

We obtained followup spectra of six of our candidate BLAPs using the William Herschel Telescope (WHT) and the SALT. Our main aim was to detect principal line features which could be used for identification purposes and possibly to constrain spectral parameters.

The data were reduced using standard procedures (see Macfarlane et al. (2017a) for more details) and an overview of the observations are given in Table 3. The bulk of the spectra were obtained using the Robert Stobie Spectrograph (RSS; Kobulnicky et al. 2003) on SALT,

Table 1. Variable stars identified in the OW survey that have a period <40 min, an amplitude >0.1 mag, and a location in the *Gaia* HRD, which is bluer than stars in the main sequence and an M_G brighter than the main white dwarf tracks. They are presented in an order of increasing period. We show their sky co-ordinates, their mean g mag; period; amplitude (from the OW data), and their parallax and distance (derived from *Gaia* EDR3). We also show the apparent M_G and de-reddened M_{G_o} absolute mag, and colours $(BP - RP)$, $(BP - RP)_o$ which are derived from *Gaia* EDR3. The values in brackets give the range of distance within the 5th and 95th percentiles and their associated range in M_G . Variable ID #7 is co-incident with OGLE-BLAP-009 (Pietrukowicz et al. 2017).

| ID | RA (J2000) | Dec. (J2000) | gow (mag) | Period (min) | Amp (mag) | π (mas) | D (kpc) | M_G | $BP - RP$ | M_{G_o} | $(BP - RP)_o$ |
|----|--|-----------------|--------------|-----------------|--------------|----------------|----------------|---------------|-----------|-----------|---------------|
| 1 | 08 ^h 20 ^m 47 ^s .2 | −33°01′07″.8 | 16.6 | 7.4 | 0.13 | 0.26 ± 0.05 | 3.7 (3.0–5.9) | 4.0 (3.0–4.5) | −0.14 | 2.7 | −0.78 |
| 2 | 18 ^h 20 ^m 14 ^s .3 | −28°50′59″.8 | 18.1 | 9.1 | 0.11 | 0.33 ± 0.14 | 2.9 (2.1–7.2) | 5.7 (3.7–6.4) | 0.40 | 4.9 | −0.02 |
| 3 | 18 ^h 12 ^m 27 ^s .9 | −29°38′48″.3 | 18.3 | 10.8 | 0.28 | 1.06 ± 0.52 | 1.4 (0.9–7.2) | 7.5 (4.0–8.5) | 0.55 | 7.0 | 0.34 |
| 4 | 18 ^h 19 ^m 20 ^s .9 | −27°29′56″.1 | 17.3 | 15.9 | 0.19 | −0.03 ± 0.12 | 5.8 (3.9–11.5) | 3.4 (1.9–4.2) | 0.22 | 1.8 | −0.57 |
| 5 | 18 ^h 11 ^m 00 ^s .2 | −27°30′13″.5 | 18.1 | 23.0 | 0.21 | 0.14 ± 0.15 | 4.2 (2.8–9.5) | 4.8 (3.0–5.7) | 0.34 | 3.5 | −0.32 |
| 6 | 18 ^h 10 ^m 38 ^s .5 | −25:16′08″.6 | 19.6 | 28.9 | 0.42 | 0.97 ± 0.38 | 1.3 (1.0–6.2) | 8.4 (5.0–9.0) | 0.69 | 8.0 | 0.48 |
| 7 | 17 ^h 58 ^m 48 ^s .2 | −27°16′53″.6 | 15.6 | 32.0 | 0.28 | 0.41 ± 0.04 | 2.4 (2.1–2.9) | 3.6 (3.2–3.9) | 0.61 | 2.9 | 0.24 |
| 8 | 18 ^h 26 ^m 28 ^s .4 | −28°12′01″.9 | 16.6 | 32.4 | 0.12 | 0.01 ± 0.08 | 6.8 (4.8–12.4) | 2.6 (1.3–3.4) | 0.62 | 1.1 | −0.17 |
| 9 | 08 ^h 15 ^m 30 ^s .8 | −34°21′23″.5 | 16.6 | 36.7 | 0.20 | 0.51 ± 0.05 | 2.0 (1.7–2.4) | 5.3 (4.9–5.6) | −0.08 | 4.4 | −0.52 |

Table 2. A log of photometric observations made using the 1.0m telescope at SAAO, Sutherland, South Africa. The last three columns show the period of the maximum peak in the LS periodogram; its amplitude (peak to peak) and its FAP.

| ID | Name | Start date | Start HJMD | End HJMD Images | No. | Exp. (s) | Filter | g (mag) | Period (min) | Amplitude (mag) | log FAP |
|----|-----------------------|------------|------------|--------------------|-----|-------------|--------|--------------|-----------------|--------------------|---------|
| 1 | OW J082047.2–330107.8 | 2021-02-17 | 59262.9151 | 59263.0773 | 468 | 30. | g | 16.7 | 7.51 | 0.107 | −115.4 |
| | | 2021-02-18 | 59263.9078 | 59264.0804 | 498 | 30. | g | 16.7 | 7.52 | 0.092 | −63.4 |
| | | 2021-02-19 | 59264.9048 | 59265.0531 | 428 | 30. | g | 16.7 | 7.58 | 0.072 | −53.1 |
| | | 2021-02-23 | 59268.7668 | 59269.0366 | 778 | 30. | g | 16.7 | 7.49 | 0.066 | −66.9 |
| 4 | OW J181920.9–272956.1 | 2016-07-30 | 57599.7074 | 57599.8229 | 162 | 60. | g | 17.4 | 15.8 | 0.186 | −52.6 |
| | | 2016-08-01 | 57601.7128 | 57602.0270 | 311 | 60. | g | 17.4 | 15.7 | 0.186 | −129.6 |
| | | 2016-08-03 | 57603.7636 | 57604.0513 | 144 | 60. | g | 17.4 | 15.7 | 0.165 | −40.9 |
| 5 | OW J181100.2–273013.5 | 2016-08-04 | 57604.7208 | 57605.0370 | 215 | 120. | g | 18.3 | 22.9 | 0.273 | −69.4 |
| | | 2016-08-05 | 57605.7191 | 57606.0507 | 238 | 120. | g | 18.3 | 22.7 | 0.210 | −46.6 |
| | | 2016-08-08 | 57608.7158 | 57608.9221 | 297 | 60. | - | - | 22.9 | 0.294 | −71.8 |
| 8 | OW J182628.4–281201.9 | 2017-05-07 | 57880.9504 | 57881.0752 | 540 | 20. | g | 16.6 | 33.0 | 0.176 | −184.9 |
| | | 2017-05-09 | 57883.0261 | 57883.1926 | 720 | 20. | g | 16.7 | 32.9 | 0.186 | −240.7 |
| 9 | OW J081530.8–342123.5 | 2021-02-20 | 59265.8426 | 59266.0604 | 628 | 30. | g | 16.6 | 36.8 | 0.193 | −318.8 |
| | | 2021-02-21 | 59266.8003 | 59267.0445 | 704 | 30. | g | 16.6 | 36.8 | 0.197 | −333.8 |
| | | 2021-02-22 | 59267.8817 | 59268.0421 | 463 | 30. | g | 16.6 | 36.8 | 0.202 | −239.9 |

Table 3. A log of spectroscopic observations showing the date, telescope, instrument, grating, slit-width, position angle, grating angle, and exposure time.

| ID | Name | Date | Telescope | Instrument | Grating | Slit-width (arcsec) | Position angle (deg) | Grating angle (deg) | Exposure (s) |
|----|-----------------------|------------|-----------|------------|-----------|------------------------|-------------------------|------------------------|-----------------|
| 1 | OW J082047.2–330107.8 | 2016-02-10 | SALT | RSS | PG0900 | 1.5 | 54 | 14.38 | 700 |
| | | 2017-11-30 | SALT | RSS | PG0900 | 1.5 | −101 | 14.38 | 804 |
| 3 | OW J181227.9–293849.3 | 2016-09-30 | SALT | RSS | PG2300 | 1.5 | 45 | 30.88 | 2 × 600 |
| 4 | OW J181920.9–272956.1 | 2016-08-05 | WHT | ISIS | 158R/300B | 1.0 | 10.8 | 58.8/58.3 | 30 × 90 |
| | | 2016-09-07 | SALT | RSS | PG2300 | 2.0 | 56 | 30.88 | 15 × 60 |
| 5 | OW J181100.2–273013.5 | 2016-05-15 | SALT | RSS | PG0900 | 1.5 | 291 | 14.38 | 1800 |
| | | 2016-10-22 | SALT | RSS | PG2300 | 1.5 | 0 | 30.88 | 720 |
| 6 | OW J181038.5–251608.6 | 2016-05-10 | SALT | RSS | PG0900 | 1.5 | 233 | 14.38 | 2200 |
| 7 | OW J175848.2–271653.6 | 2016-06-28 | SALT | RSS | PG0900 | 1.5 | 177 | 14.38 | 50 × 30 |
| | | 2016-07-09 | SALT | RSS | PG0900 | 1.5 | 177 | 14.38 | 50 × 30 |
| 9 | OW J081530.8–342123.5 | 2017-11-18 | SALT | RSS | PG0900 | 1.5 | −99 | 14.38 | 840 |
| | | 2021-05-01 | SALT | RSS | PG0900 | 1.5 | 98 | 14.38 | 6 × 400 |
| | | 2021-05-02 | SALT | RSS | PG0900 | 1.5 | 99 | 14.38 | 6 × 400 |
| | | 2021-05-09 | SALT | RSS | PG0900 | 1.5 | 99 | 14.38 | 6 × 400 |

using either the PG0900 or the PG2300 grating. The former covered a wavelength range of ~ 3980 – 6980 Å with a dispersion of 0.97 Å, whereas the latter covered the wavelength range of ~ 3900 – 4950 Å with a dispersion of 0.34 Å.

All objects show Balmer lines in absorption with some showing helium lines (see Fig. 1). Atmospheric parameters such as effective

temperature, T_{eff} , surface gravity, $\log g$, helium abundance, $\log y = \log \frac{n(\text{He})}{n(\text{H})}$ were determined by fitting the rest-wavelength corrected Balmer and helium lines using the FITSB2 routine (Napiwotzki et al. 2004). Two grids of model atmospheres were used, which cover wide ranges in parameter space. Both model grids were constructed by combining LTE calculation of the atmospheric stratification with

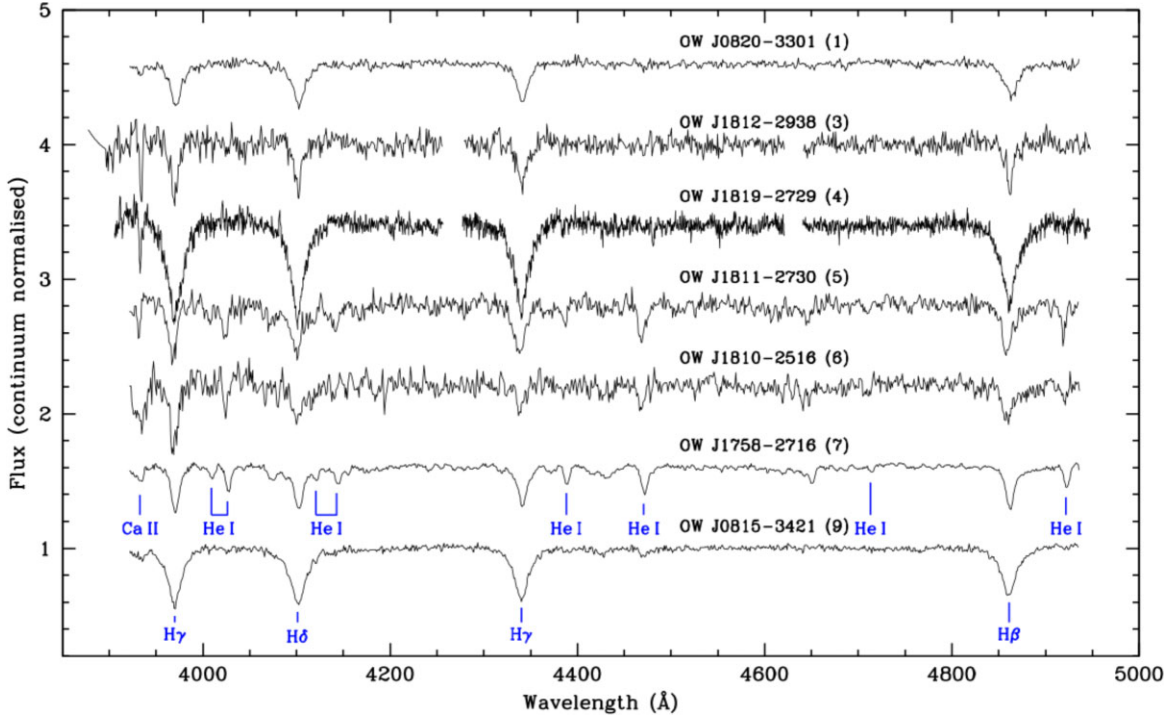


Figure 1. The continuum normalized SALT spectra of our targets where each spectrum has been shifted by +0.5 flux units. We note the wavelength of key lines in the spectra.

the ATLAS12 code (Kurucz 1996), including full line-blanketing, and of NLTE occupation densities for extensive hydrogen and helium model atoms with the DETAIL code (Giddings 1981). The emergent optical hydrogen and helium lines spectrum was finally synthesized with the SURFACE code (Butler & Giddings 1985; Przybilla, Nieva & Butler 2011), using state-of-the-line broadening tables. Recent updates and extensions of the codes are described in Irrgang et al. (2018). ATLAS12 allows individual non-solar abundance pattern to be implemented. The first grid of models uses an abundance pattern typical for sdB stars (Naslim et al. 2013; additional details can be found in Schaffenroth et al. 2021). The grid covers the temperature range $T_{\text{eff}} = 9000\text{--}55\,000$ K, surface gravities from $\log g = 4.6$ to 6.6, and helium to hydrogen ratio y from 10^{-4} to 10 times that of the sun.

Another grid was provided by Hämmerich (private communication) with models covering helium-to-hydrogen abundance ratio from 10^{-4} to five times that of the sun, but using the solar metal abundance pattern, which allowed the range for the surfaces gravities to be extended to $\log g = 4.0$, which was necessary for three program stars.

5 INDIVIDUAL OBJECTS

5.1 OW J082047.2–330107.8

The OW photometric observations of OW J082047.2–330107.8 (ID 1 in Table 1, and hereafter referred to as OW J0820–3301) showed evidence for periodic modulation on a period of 7.4 min and 0.13 mag in amplitude. We obtained followup photometry on four nights in 2021 February (Table 2), with a significant periodic signal on a period of 7.5 min on each occasion. The amplitude appears to be variable as does the significance of the period. In Fig. 2, we show these light curves: the amplitude of the modulation does change

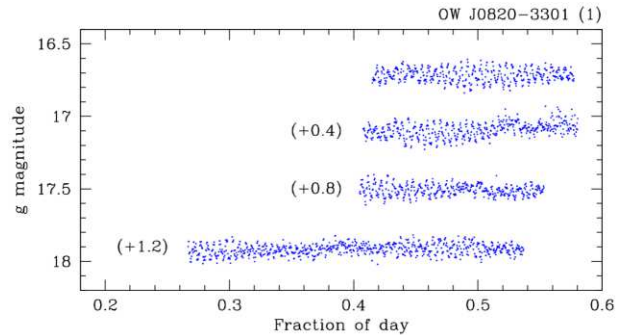


Figure 2. Light curves of OW J0820–3301 obtained with the SAO 1m telescope. The top light curve is shown at the correct brightness, whereas subsequent light curves (top to bottom) are displaced for display purposes only.

over time. An LS power spectrum (Fig. 3) shows an additional, less prominent, peak corresponding to a shorter period (5.7 min).

The multiperiodic nature of OW J0820–3301, and its high temperature (Table 5) are consistent with the properties of V361 Hya (or EC 14026) variables (Kilkenny et al. 1997; Heber 2016; Lynas-Gray 2021). Pulsation amplitudes in V361 Hya variables are typically less than 1 per cent compared with nearly 10 per cent in OW J0820–3301. However, several other V361 Hya variables have been observed with significant semi-amplitudes, including PG 1605+072 ($P = 8.0$ min, $a \sim 0.064$ mag; Koen et al. 1998), Balloon 090100001 ($P = 5.9$ min, $a \sim 0.060$ mag; Baran et al. 2009), and CS 1246 ($P = 6.2$ min, $a \sim 0.025$ mag; Barlow et al. 2010).

Interestingly, the large amplitude oscillation observed in CS 1246 decayed to $a < 0.005$ mag in the following 8 yr (Hutchens et al. 2017), while amplitude variations appear to be important in other V361 Hya variables (Reed et al. 2004; Kilkenny 2010).

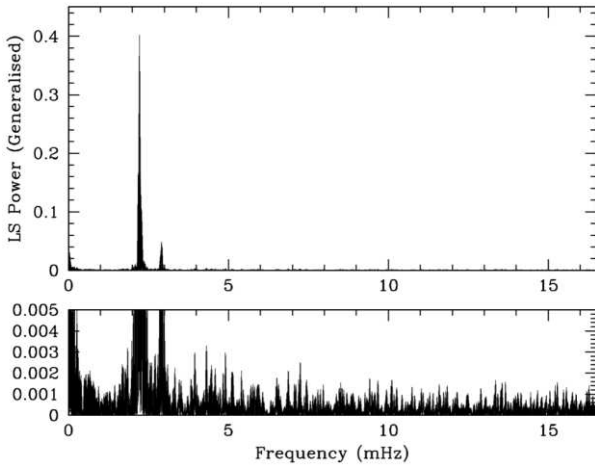


Figure 3. Generalized LS power spectrum of OW J0820-3301.

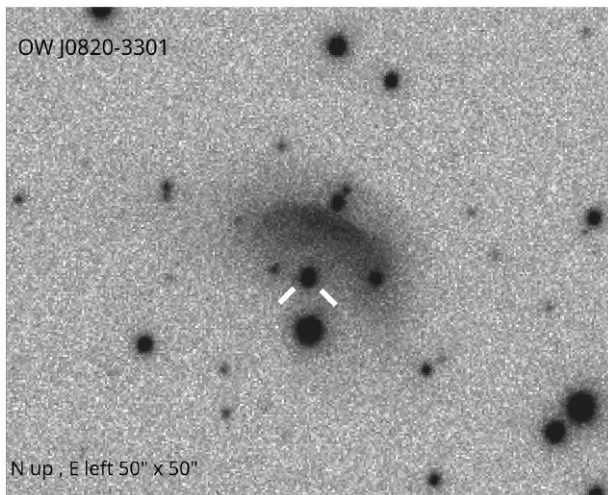


Figure 4. An image of the immediate field of OW J0820-3301 in $H\alpha$, combining three exposures taken during the VPHAS+ survey (Drew et al. 2014). It is 50×50 arcsec² wide and the target is in the centre, indicated by the white dashes. An extended nebula lies to the north of OW J0820-3301.

The SALT spectrum of OW J0820-3301 obtained in 2016 (see details in Table 3) showed a nebular spectrum of a Strömgren sphere superimposed on broader Balmer absorption lines. After careful sky subtraction, the emission line spectrum was separated from the stellar spectrum. The latter is shown in Fig. 1. Fitting this spectrum indicates that OW J0820-3301 has a temperature of $T_{\text{eff}} \sim 37\,400$ K and $\log g \sim 5.7$ (Table 5).

We performed a search for extended emission around our targets using the AAO/UKST $H\alpha$ ¹ and VPHAS+ (Drew et al. 2014) surveys and extracted an image for all sources. We found evidence for extended emission from around OW J0820-3301: in Fig. 4 we show an image taken in $H\alpha$ extracted from the VPHAS+ survey (Drew et al. 2014) which has higher resolution. The DECaPS survey² shows the nebula as prominently in green colour, indicative of strong O III or $H\beta$ emission. Without more detailed spectroscopic observations across the nebula (and ideally integral field unit observations), we are

¹<http://www-wfau.roe.ac.uk/ss/halpha>

²<http://decaps.skymaps.info>

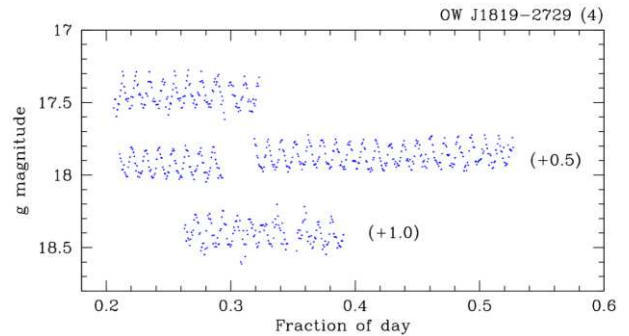


Figure 5. Light curves of OW J1819-2729 obtained with the SAAO 1m telescope.

unable to be certain that the nebula is associated with OW J0820-3301. However, using statistical arguments, we can determine the likelihood that two ‘interesting’ objects are located within (say) 2 arcsec of each other. The *Gaia* EDR3 catalogue (Gaia Collaboration 2021) shows 56 stars within 1 arcmin radius of OW J0820-3301 that are brighter than $G < 19$ mag (85 for $G < 20$ mag). The probability that this is a chance alignment is 0.03 per cent ($G < 19$) and 0.07 per cent.

If OW J0820-3301 and the nebula are associated, then we can estimate the age of the nebula. The *Gaia* EDR3 data (Gaia Collaboration 2021) has a best-fitting distance to OW J0820-3301 of 3.7 kpc. The $H\alpha$ image shows a nebula which has a diameter along its semimajor axis of ~ 8 arcsec. For a distance of 3.7 kpc, simple geometry indicates a semimajor axis of ~ 0.14 pc. If we assume a velocity of the expanding material to be $10\text{--}40$ km s⁻¹ (Corradi & Schwarz 1995), we find an age of the nebula of $\sim 3400\text{--}13\,600$ yr. More dedicated spectroscopic observations of the nebula are required.

5.2 OW J181227.9-293848.3

We identified OW J181227.9-293848.3 (ID 3 in Table 1, and hereafter referred to as OW J1812-2938) as having a very significant peak in its power spectrum at 10.8 min and an amplitude of 0.28 mag. No followup photometry was obtained of this source but we did obtain two spectra using SALT in 2016 (Table 3). We show the combined normalized spectrum in Fig. 1 that shows Balmer lines in absorption and a prominent Ca II absorption line.

Fitting this spectrum indicates that OW J1812-2938 has a temperature $T_{\text{eff}} \sim 31\,000$ K and $\log g \sim 4.7$ (Table 5). These results, together with its period and amplitude, place it in the parameter range consistent with it being a BLAP, and we therefore designate it OW-BLAP-1.

5.3 OW J181920.9-272956.3

We identified OW J181920.9-272956.3 (ID 4 in Table 1, and hereafter referred to as OW J1819-2729) as having a very significant peak in its power spectrum at 15.7 min and an amplitude of 0.19 mag. We obtained followup photometry of this source using the SAAO 1.0m telescope on three nights with multiple 60 s exposures on each occasion (cf Table 2). The light curves are shown in Fig. 5. These data confirm the 15.9 min period found from OW data; although, there is also a peak in the power spectra at half the 15.9 min period. There are some side-lobes of the main peak on the night of 2016 August 03 but this has the smallest number of photometric points. The folded light curves are sinusoidal and symmetric.

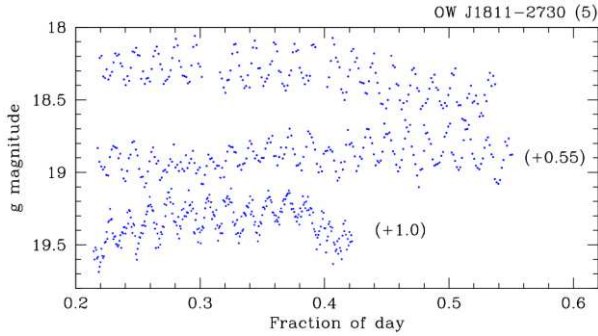


Figure 6. Light curves of OW J1811–2730 obtained with the SAAO 1m telescope.

We obtained spectra of OW J1819–2729 using SALT, SAAO 1.9m telescope, and WHT. The longest series was obtained using the WHT where a series of 30 low-resolution spectra were obtained. They were obtained at relatively high airmass (1.8–2.0) and the individual spectra were of low signal-to-noise ratio. However, the co-added spectra revealed Balmer absorption lines, with only marginal evidence for helium lines. The ratio of the equivalent width (Ca II H+K, He ϵ) is consistent with an A-type spectrum.

The temperature ($T_{\text{eff}} \sim 12\,300$ K) derived from the spectral fits (Table 5) is the lowest of the stars in our sample and is similar to the pulsating sdA stars (Bell et al. 2018). However, there is only one star in the Bell et al. (2018) set of new stars that has a period (4.6 min), which is even remotely close to that seen here but the amplitude of the pulsation of that star is <0.4 per cent. These observations indicate that OW J1819–2729 is a possible sdAV variable star.

5.4 OW J181100.2–273013.3

OW J181100.2–273013.3 (ID 5 in Table 1, and hereafter referred to as OW J1811–2730) was observed on three occasions using the SAAO 1.0m telescope: at two epochs the exposure times were 120 s and at one epoch 60 s (Table 2). The light curves from the individual nights are shown in Fig. 6.

The period derived from each of the three nights is 22.7–22.9 min with an amplitude in the range 0.21–0.29 mag, which is fully consistent with the 23.0 min and 0.21 mag from the OW survey data. To search for other periods in the light curve, we removed global trends in each night (which may have been due to differential colour terms between the comparison stars) and obtained an LS power spectrum (Fig. 7). There is evidence for the peaks in the power spectrum being split, but these largely disappear after pre-whitening on the period with peak power. We conclude that there is little evidence for a second period in this source.

The mean spectrum shown in Fig. 1 shows the Balmer lines in absorption together with He I also in absorption. The spectral fits (Table 5) indicates that OW J1811–2730 has a temperature $T_{\text{eff}} \sim 27\,000$ K and $\log g \sim 4.8$. Together with the photometric properties indicates that OW J1811–2730 is a BLAP and we designate OW-BLAP2.

5.5 OW J181038.5–251608.6

We identified OW J181038.5–251608.6 (ID 6 in Table 1, and hereafter referred to as OW J1810–2516) as having a very significant peak in its power spectrum at 28.9 min and an amplitude of 0.42 mag. At $g = 19.6$ mag, it is the faintest target in our sample. We

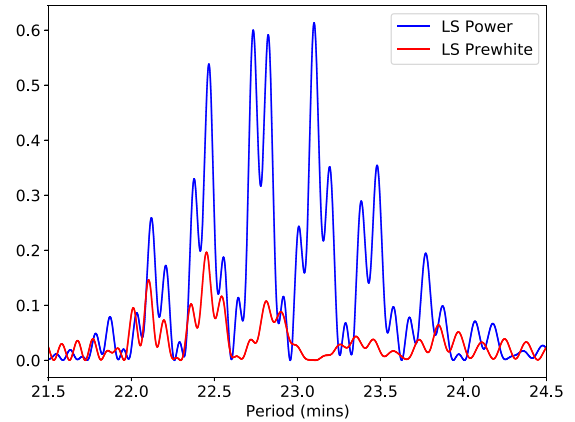


Figure 7. The LS power spectrum of the combined light curve of OW J1811–2730 (after global trends have been removed) and the LS power spectrum after the light curve has been pre-whitened by removing the period with maximum power.

obtained one spectrum of OW J1810–2516 using SALT and the RSS and its normalized spectrum is shown in Fig. 1. Balmer lines are seen in absorption as are several lines due to helium. The fits to the spectra (Table 5) indicate a temperature $T_{\text{eff}} \sim 30\,000$ K and $\log g \sim 4.2$. Together with the period and amplitude, we identify this as a BLAP and name it OW-BLAP-3.

5.6 OW J175848.2–271653.6

OW J175848.2–271653.6 (ID 7 in Table 1, OW J1758–2716) was reported as a variable with a period of 32.5 min and amplitude of 0.25 mag (Macfarlane et al. 2017a). The folded light curve indicated that the source was similar to that of δ Sct stars. However, an optical spectrum indicated the star was more similar to a B spectral type than an A-F spectral type, which would be expected from a δ Sct star. Intriguingly, the phase folded light curve showed a curious ‘notch’ at peak brightness: we display the data reported in Macfarlane et al. (2017a) folded on the main period in Fig. 8. Macfarlane et al. (2017a) made the comparison between the notch observed here with the ‘Bump Cepheids’ (Mihalas 2003). We obtained an additional set of 50 spectra taken on two nights in 2016 (see Table 3). Fitting the mean spectrum, we find $T_{\text{eff}} \sim 27\,000$ K and $\log g \sim 4.2$ (Table 5) and conclude that OW J1758–2716 is a BLAP and name it OW-BLAP-4.

5.7 OW J182628.4–2812019

OW J182628.4–2812019 (ID 8 in Table 1, OW J1826–2812) was observed on two nights in May 2017 (Table 2) using the 1.0m telescope and SHOC. The period which we determine (32.9–33.0 min) is slightly longer than found using the original OW data (32.4 min) and with a higher amplitude (~ 0.18 mag compared to 0.12 mag). We show the light curves in Fig. 9 and the phase folded binned light curve in Fig. 8. There is a curious ‘ledge’ like feature just before maximum light. We return to this in Section 6. Spectroscopic observations are still required to determine the nature of this source.

5.8 OW J081530.8–342123.5

OW J081530.8–342123.5 (ID 9 in Table 1, and hereafter referred to as OW J0815–3421) has the longest apparent period of the candidate BLAPs shown in Table 1 (36.7 min) and an amplitude of 0.20 mag.

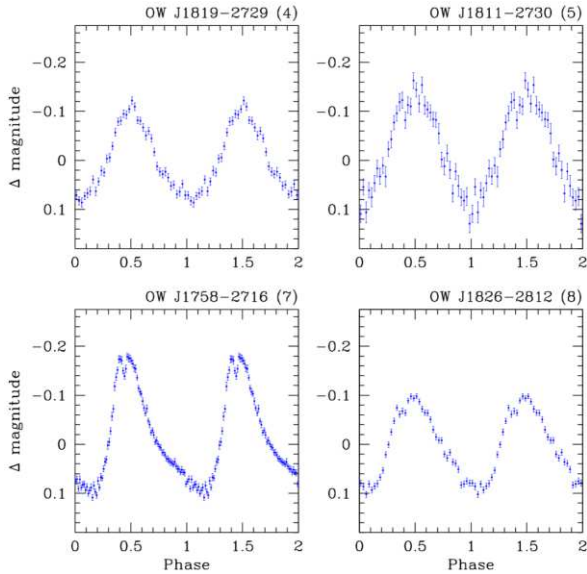


Figure 8. The phased and averaged light curves of OW J1819–2729 ($P = 15.715$ min, top left), OW J1811–2730 ($P = 22.915$ min, top right), OW J1758–2716 ($P = 32.00$ min, bottom left), and OW J1826–2812 ($P = 32.960$ min, bottom right).

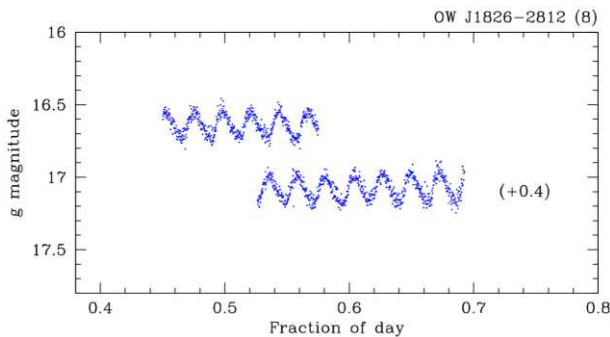


Figure 9. Light curves of OW J1826–2812 obtained using the SAO 1m telescope.

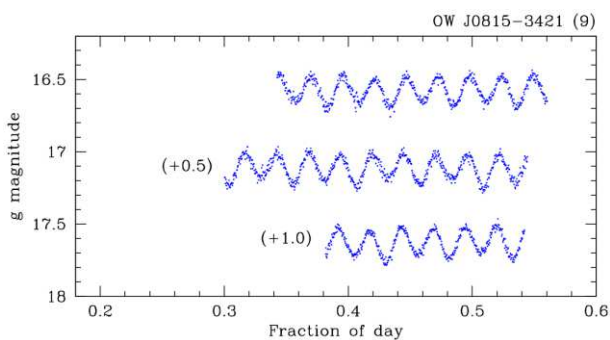


Figure 10. Light curves of OW J0815–3421 obtained with the SAO 1m telescope.

Followup photometric observations were obtained on three nights in February 2021 (Table 2). A strong periodic signal was seen in the light curves with the LS periodogram indicating a period of 36.8 min, which is consistent with the OW period. However, in Fig. 10, we show the individual light curves from these nights: there is evidence that

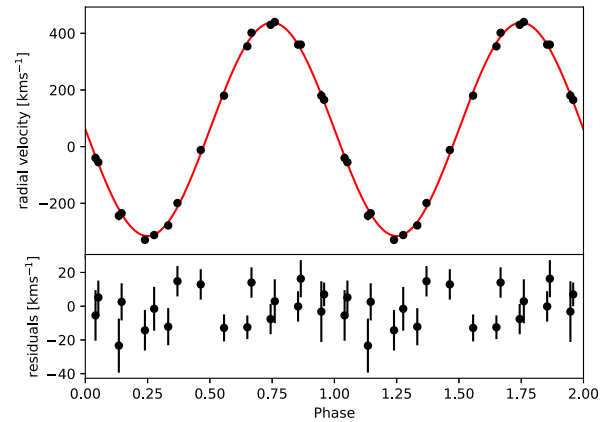


Figure 11. Upper panel: the radial velocity data of OW J0815–3421 phased on the binary orbital period of 73.7 min together with the best-fitting sinusoid. Lower panel: the residuals to the fit. Two orbits are shown for better visualization.

the depth of every second minimum is deeper than the preceding minimum. This suggests that the true period, possibly an orbital ellipsoidal modulation, is 73.6 min.

We obtained a single spectrum of OW J0815–3421 in 2017 (Table 3) that showed the Balmer series in absorption (Fig. 1). A fit to this spectrum indicates a temperature and gravity consistent with that of an sdB star. To search for radial velocity variations, we obtained a series of spectra using SALT in May 2021. This revealed a clear radial velocity variation (a semi-amplitude of 376 ± 15 km s^{-1}) on a period of 73.6 min: we show the phase-folded radial velocity curve in Fig. 11. A fit to the combined spectrum (made after accounting for the radial velocity variation of the individual spectra) indicates a temperature $T_{\text{eff}} = 26,500 \pm 1000$ K, and $\log g = 5.68 \pm 0.15$.

We can now use this information to model and constrain the resulting stellar parameters using the photometric light curve, using *Lcurve*,³ [see Copperwheat et al. (2011) for a detailed description]. To model the system, we use a spherical star for the white dwarf and use a Roche geometry for the sdB companion. The free parameters in the model are the period (P), time of inferior conjunction (t_0), mass-ratio (q), inclination (i), the radii scaled by the semimajor axis ($r_{1,2}$), the effective temperature of both components ($T_{\text{eff},1,2}$), and the velocity scale ($[(K_1 + K_2) \sin i^{-1}]$).

Ellipsoidal variations alone are not sufficient to fully constrain the binary parameters, and we therefore add priors and other model constraints. We use Gaussian priors on the sdB temperature as derived from the spectroscopy, surface gravity, and radial velocity semi-amplitude. We fix the limb and gravity darkening parameters using the tabulated values by Gianninas et al. (2013) and fix the beaming exponent to 1.62 (Loeb & Gaudi 2003; Bloemen et al. 2011). For the white dwarf, we use the approximation of the mass–radius relation of Eggleton from Verbunt & Rappaport (1988) to constrain the radius. First, the white dwarf radius cannot be smaller than the mass–radius relation. Secondly, we use a Gaussian prior to constrain the relative size of the white dwarf compared to the zero-temperature white dwarf relation to 10 per cent. To find the best parameter values and uncertainties, we use a Markov Chain Monte Carlo method as implemented in EMCEE (Foreman-Mackey

³<https://github.com/trmrsh/cpp-lcurve>

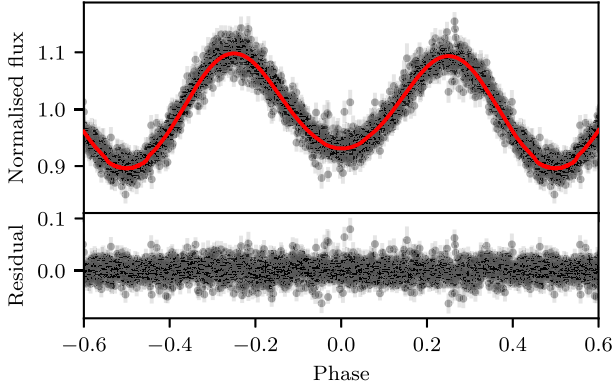


Figure 12. The data of OW J0815–3421, shown in black, has been phased on a period of 73.71 min. The red solid line shows the fit to the data made using `Lcurve`. The data have been repeated to cover two cycles and phase 0.0 represents the secondary minimum.

Table 4. The system parameters derived for OW J0815–3421 using `Lcurve` to model the light curve.

| | |
|---------------------|-------------------------------|
| t_0 (HJD) | 2459267.432196(26) |
| P (d) | 0.0511843(16) |
| q | $0.493^{+0.061}_{-0.072}$ |
| i ($^\circ$) | $83.14^{+4.60}_{-10.55}$ |
| M_1 (M_\odot) | $0.707^{+0.086}_{-0.082}$ |
| M_2 (M_\odot) | $0.343^{+0.076}_{-0.066}$ |
| R_1 (R_\odot) | $0.01189^{+0.0012}_{-0.0011}$ |
| R_2 (R_\odot) | $0.216^{+0.018}_{-0.015}$ |
| a (R_\odot) | $0.590^{+0.027}_{-0.027}$ |
| T_1 (K) | 14077^{+11290}_{-6233} |
| T_2 (K) | 26461^{+1052}_{-965} |
| $\log g_2$ | $5.44^{+0.021}_{-0.028}$ |

et al. 2013). Before we fitted the model, we detrended and rescaled the uncertainties of the three individual light curves. We fit the combined light curve using 512 walkers and 2000 generations and show the resulting best fit and the folded light curve in Fig. 12, and the resulting best-fitting parameters with their associated errors in Table 4.

The mass of the white dwarf is $\sim 0.7 M_\odot$ ($T_{\text{eff}} \sim 14\,000$ K) while the mass of the sdB star is $\sim 0.34 M_\odot$ ($T_{\text{eff}} \sim 26\,500$ K). The component masses and orbital period of (73.7 min) make it similar to the well-known white dwarf, sdB binary CD–30° 11223, which has an orbital period of 70.5 min (Vennes et al. 2012) and PTF1 J2238+7430, the recently discovered white dwarf, sdB binary (Kupfer et al. 2022). The recent catalogue of post-common envelope binaries of Kruckow et al. (2021) lists five white dwarf, sdB binaries with an orbital period shorter than 80 min: OW J0815–3421 is now the sixth such binary. The mass of the component stars are similar to ZTF J2320+3750 (55.25 min; Burdge et al. 2020a) and ZTF J2055+4651 (56.35 min; Kupfer et al. 2020).

The finding that OW J0815–3421 is a binary indicates that medium-resolution spectroscopic observations made over several days could reveal evidence for binarity in the other sources identified in this survey [cf. the comments of Byrne & Jeffery (2020) on the Roche lobe overflow model for the formation of BLAPs].

6 DISCUSSION

Of the nine sources which we identified as candidate BLAPs (Table 1), four have characteristics consistent with being a BLAP. The key was obtaining spectra with sufficient spectral resolution ($R \sim 2000$) to be able to fit the absorption lines and hence obtain sufficiently constrained values for temperature and gravity. Followup high-time-resolution photometry was essential in identifying OW J0815–3412 as a very short-period binary containing a sdB star and also identifying the notch feature in four objects, two of which are BLAPs. We note that the derived periods from followup photometry are consistent with the initial periods derived from the OW survey. We now discuss all sources reported in this study in the wider context.

6.1 Comparison of BLAPs with other short-period variables using the *Gaia* HRD

The simplest and most readily available means of comparing the colour and luminosity of different types of sources is through the *Gaia* HRD based on $((BP - RP), MG)$ data. Since the OW and the ZTF surveys observed fields close to the Galactic plane, the extinction can be high and can show changes on relatively small spatial scales (< 1 arcmin). We therefore de-redden the *Gaia* $((BP - RP), MG)$ data of variable stars of different types using `Bayestar19` (Green et al. 2019).

There are a number of different classes of variable stars which lie in the region of the *Gaia* HRD where BLAPs have been found (Ramsay 2018; McWhirter & Lam 2022). For instance, strongly magnetic Cataclysmic Variables (also known as Polars) can show high (up to 1 mag) variation over their orbital period, but their orbital periods are $\gtrsim 80$ min. In contrast, the interacting double degenerate that AM CVn binaries have orbital periods $\lesssim 1$ h but have amplitudes < 0.1 mag. We therefore include for comparison a number of short-period binaries ($6.9 < P_{\text{orb}} < 56.4$ min), which consist of degenerate stars and can show high amplitudes of variability, many of which also show eclipses (Burdge et al. 2020a, b) and a small sample of high amplitude sdB stars⁴ that have high amplitudes and short periods. In addition, we add the high-gravity BLAPs reported by Kupfer et al. (2019) and also the high-gravity ‘sdB’ pulsators reported in Kupfer et al. (2020). Since the periods of these systems are similar, with the latter sample showing only slightly lower amplitudes, we class both these samples as high-gravity BLAPs, although they may have a different internal structure. We also take the sources originally reported by Pietrukowicz et al. (2017) and have $\text{Dec.} > -30^\circ$ and hence the reddening can be determined using `Bayestar19`. In Fig. 13, we show the location of these stars in the $((BP - RP)_o, M_{G_o})$ plane and for comparison stars which are within 50 pc of the Sun, which we assume have negligible reddening.

As can be seen, the sources cover a wide range in the *Gaia* HRD, encompassing the area bluer than the main sequence but more luminous than the main white dwarf cooling tracks. The BLAPs have a wide range of M_{G_o} , although we caution that because the error on their parallax is generally high and the resulting uncertainty on M_{G_o} can be up to ~ 1 mag (cf. Table 1). The compact binaries tend to be less luminous compared to the other classes with those being more luminous having an sdB star as a binary component. Stellar pulsators appear to be more luminous. However, it is not possible to determine

⁴PG 1605+072, Balloon 90100001, PG 1716+426, BPS BS 16559–0077, PB 7032

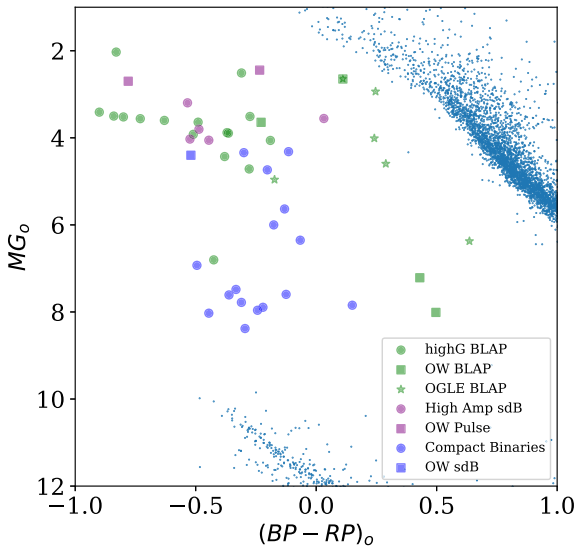


Figure 13. The observed $(BP - RP)_o$, MG_o colour-absolute magnitudes for the BLAPs and other high amplitude pulsators as identified in the OW survey. For comparison, we also show the position of the high-gravity BLAPs reported in Kupfer et al. (2019, 2021); compact binaries identified in Burdge et al. (2020a, b); and high amplitude sdB stars.

the nature of any given source based on its location purely in the *Gaia* HRD.

Fortunately, for seven of the sources in this study, we have been able to determine their temperature and gravity (Table 5). In Fig. 14, we show the location of the OW BLAPs, the BLAP sample from Pietrukowicz et al. (2017), and the high-gravity BLAPs from Kupfer et al. (2019). We also show the evolutionary tracks for stars of different mass taken from Kupfer et al. (2019). The OW BLAPs share a similar part of the T_{eff} , $\log g$ plane (relatively low gravity) while the high-gravity BLAPs have a shorter pulsation period and high gravity.

6.2 Notch feature at maximum brightness

Macfarlane et al. (2017a) identified a dip in the light curve of OW J1758–2716 occurring near maximum light, which was compared to features seen in ‘Bump’ Cepheid variables. These bumps are featured in the phase-folded light curve that occur on the rise to maximum brightness or in the descent from brightness. The phase of where this occurs is known as the Hertzsprung Progression (Hertzsprung 1926; Bono, Marconi & Stellingwerf 2000) and depends on stellar mass, and therefore the observed period. There are Cepheids that show a dip at flux maximum very similar to what we observe in OW J1758–2716, see for example RU Dor (fig 9, Plachy et al. 2021). It is likely that Bump features are due to a resonance between the fundamental pulsation mode and the second overtone (e.g. Gastine & Dintrans 2008 and references therein).

We do not have additional photometric observations since those reported by Macfarlane et al. (2017a), which showed photometry covering a timeline of ~ 160 min. Further observations would be required to search for a second over-tone in the light curve. However, as shown in Fig. 8, OW J1811–2730 and OW J1826–2812 show hints for a slight bump in their folded light curves on the rise to maximum brightness. There is no sign of bump features in the high-gravity BLAPs identified by Kupfer et al. (2019).

6.3 sdA pulsators

High-gravity A stars (sdA’s) have been widely discussed since being identified in the Sloan Digital Sky Survey with H-dominated spectra, $9000 > T_{\text{eff}} > 6500$ K, and $6.5 > \log g > 5.5$ (Kepler et al. 2016). While purely a spectroscopic classification, they have been identified with binaries of a subdwarf and a main-sequence object of type FGK; main-sequence A stars with a high-surface gravity; or extremely low-mass white dwarfs (ELMs) or their precursors (pre-ELMs). Of these, only the latter (ELMs and pre-ELMs) stand scrutiny (Pelisoli et al. 2016; Bell et al. 2018).

Bell et al. (2018) in their search for pulsating sdA stars found three pre-ELM candidates that have temperatures (~ 8000 K) which are slightly cooler than that measured for OW J1819–2729. They indicate that pre-ELM stars might undergo CNO flashes on a short time-scale. Byrne & Jeffery (2020) studied the pulsation properties of pre-ELMs and ELMs as they evolve from the subgiant branch, where they must lose mass to a close companion, on to the ELM white dwarf sequence. Their models included chemical diffusion, and demonstrated how opacity from concentrated iron-group elements can switch on pulsations in pre-ELM models exactly where BLAPs had previously been identified (Pietrukowicz et al. 2017; Kupfer et al. 2019). A few models with core masses $0.255 \leq M_{\text{core}} \leq 0.305 M_{\odot}$ show a late hydrogen-shell flash after becoming an ELM. This flash inflates the white dwarf causing a loop in the evolution track which passes through the T_{eff} , $\log g$ plane in the region occupied by OW J1819–2729. During this time, the models are also unstable to pulsation, with periods approximately between 200 and 4000 s ($\log g$ between 6.0 and 4.0).

Difficulties with this argument include the short time that models spend in such flash-driven loops, and the expectation that, in order to become an ELM, the agency of a companion is required. Nevertheless, further evidence to test the notion that OW J1819–2729 is a shell-flashing ELM should be sought.

6.4 Space density of BLAPs

The OW survey covered 404 distinct fields each covering 1 square degree. We have identified four stars which have short photometric periods and high amplitudes with followup spectroscopic observations indicate they are BLAPs, implying one BLAP per $\sim 0.01 \text{ deg}^{-2}$. Byrne et al. (2021) made predictions of how many BLAPs would be expected in our Galaxy using the Binary Population Spectral Synthesis code (Eldridge et al. 2017). They found the numbers were very dependent on Galactic latitude (concentrated towards the plane) and longitude (highest the Bulge) although regions of high extinction could make this very variable. Regions with the highest concentrations of predicted BLAPs reach $\sim 0.3 \text{ deg}^{-2}$ at a depth of $g = 20$ mag, but a median of 0.001 deg^{-2} at $b = 0^\circ$. Moving to $b = 15^\circ$ results in a very low number of BLAPs being predicted. Our search for BLAPs in the OW survey did not reach as faint as $g = 20$ mag but with an observed number density of $\sim 0.01 \text{ deg}^{-2}$ down to $g \sim 19$, our findings appear reasonably consistent with the predictions of Byrne et al. (2021), giving good grounds to suggest that 12 000 BLAPs may exist in our Galaxy.

7 CONCLUSION

We have used data taken as part of the OW survey to search for short-period, high amplitude variables, which may be BLAPs: we identified nine stars that we initially classed as candidate BLAPs. Using a combination of followup photometry, spectroscopy, and *Gaia*

Table 5. The results of spectral fits to optical spectra of the candidate BLAPs, including the best-fitting effective temperature, surface gravity, and helium-to-hydrogen abundance ratio. The penultimate column shows the likely variable star classification.

| ID | Name | T_{eff} (K) | $\log g$ | $\log n_{(\text{He}/\text{H})}$ | Classification | New designation |
|----|---------------|----------------------|-----------------|---------------------------------|----------------|-----------------|
| 1 | OW J0820-3301 | $37\,400 \pm 1500$ | 5.71 ± 0.11 | -2.5 ± 0.3 | V361 Hya | |
| 3 | OW J1812-2938 | $30\,600 \pm 2500$ | 4.67 ± 0.25 | -2.1 ± 0.2 | BLAP | OW-BLAP-1 |
| 4 | OW J1819-2729 | $12\,300 \pm 500$ | 4.81 ± 0.20 | -0.6 ± 0.2 | sdAV | |
| 5 | OW J1811-2730 | $27\,300 \pm 1500$ | 4.83 ± 0.20 | -0.7 ± 0.1 | BLAP | OW-BLAP-2 |
| 6 | OW J1810-2516 | $29\,900 \pm 3500$ | 4.16 ± 0.40 | -0.8 ± 0.3 | BLAP | OW-BLAP-3 |
| 7 | OW J1758-2716 | $27\,300 \pm 2000$ | 4.20 ± 0.20 | -0.8 ± 0.2 | BLAP | OW-BLAP-4 |
| 9 | OW J0815-3421 | $26\,500 \pm 1000$ | 5.68 ± 0.15 | -2.8 ± 0.2 | sdB | |

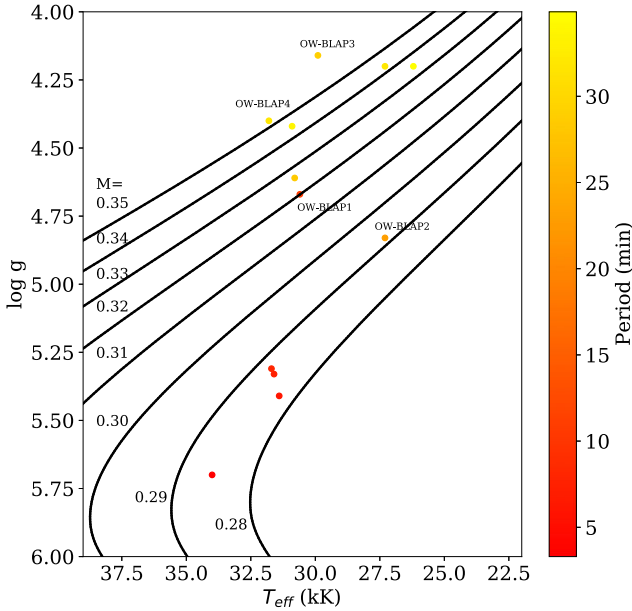


Figure 14. The solid lines are predicted evolutionary tracks for BLAPs in the T_{eff} , $\log g$ plane and taken from Kupfer et al. (2019) for stars of different masses. The BLAPs identified in the OW survey are indicated where the colour of the symbol indicates the stars pulsation period. The shorter period BLAPs come from the sample of Pietrukowicz et al. (2017) while the longer period (and high gravity) systems are from the sample of Kupfer et al. (2019). The OW BLAPs share a similar part of the plane as the lower gravity sample of Pietrukowicz et al. (2017).

data, we were able to identify four of these variables as BLAPs, one of these being previously identified as a BLAP by Pietrukowicz et al. (2017). Overall they have similar properties to the BLAPs identified by Pietrukowicz et al. (2017) rather than the high-gravity BLAPs identified by Kupfer et al. (2019, 2021).

We have also identified OW J0815–3421 as a binary system containing an sdB and a low-mass star. With an orbital period of 73.7 min, it is one of half a dozen white dwarf – sdB star binaries with orbital periods shorter than 80 min. A more detailed investigation is required to determine if it is a double-detonation thermonuclear supernova progenitor like PTF1 J2238+7430 (Kupfer et al. 2022). OW J1819–2729 is a pulsating sdAV star which has interesting properties, which makes future modelling an interesting future study. One further source, OW J0820–3301, is a V361 Hya pulsator that has an extended nebula, which is spatially nearby. Although, at this point, we cannot be certain if it is physically associated with the short-period variable. Further observations using an integral field spectrograph maybe able to determine if there is any association between the nebula and the variable star.

Finally, we note that high cadence observations of these short-period variable stars have revealed detailed structure in their folded light curve. We make comparison with other types of pulsating variable stars which show similar features in their light curves. We encourage stellar modellers to reproduce such features using appropriate models.

ACKNOWLEDGEMENTS

The targets identified in this paper were identified in data obtained using the ESO VST and OmegaCam under proposals: 088.D-4010; 090.D-0703; 091.D-0716; 092.D-0853; 093.D-0753; 093.D-0937; 094.D-0502; 095.D-0315; 096.D-0169; 097.D-0105; 098.D-0130; 099.D-0164; and 0100.D-0066. SALT spectroscopic data were obtained under proposals: 2015-2-SCI-035; 2016-1-DDT-004; 2016-1-MLT-010; 2016-1-SCI-015; and 2017-2-SCI-051. This paper uses observations made at the South African Astronomical Observatory and the South African Large Telescope, and we thank the staff for their expertise in obtaining these data. Based on observations made with the WHT (programme ID: W/16B/N4) operated on the island of La Palma by the Isaac Newton Group of Telescopes in the Spanish Observatorio del Roque de los Muchachos of the Instituto de Astrofísica de Canarias. PAW acknowledges support from UCT and the NRF. TK acknowledges support from the National Science Foundation through grant AST #2107982, from NASA through grant 80NSSC22K0338, and from STScI through grant HST-GO-16659.002-A. PJG acknowledges support from NOVA for the original OmegaWhite observations in the Dutch VST/Omegacam GTO observations. PJG is supported by NRF SARChI Grant 111693. Armagh Observatory and Planetarium is core funded by the Northern Ireland Executive through the Department for Communities. UH and AI acknowledge funding by the Deutsche Forschungsgemeinschaft (DFG) through grants HE1356/70-1 and HE1356/71-1. We thank Kinwah Wu for a useful discussion on probabilities of stars being spatially nearby and Evan Bauer who generated the evolutionary tracks shown in Fig. 14. We thank Steven Hämmerich for providing us with synthetic spectra for solar metal composition. We thank the referee for a useful report.

DATA AVAILABILITY

The images obtained as part of the OW survey can be accessed through the ESO portal. Light curves and spectra can be obtained via a reasonable request from the authors.

REFERENCES

- Alard C., Lupton R. H., 1998, *ApJ*, 503, 325
Astraatmadjam T. L., Bailer-Jones C. A. L., 2016, *ApJ*, 833, 119

- Bailer-Jones C. A. L., 2015, *PASP*, 127, 994
- Baran A. et al., 2009, *MNRAS*, 392, 1092
- Barlow B. N. et al., 2010, *MNRAS*, 403, 324
- Bell K. J. et al., 2018, *A&A*, 617, A6
- Bellm E. C. et al., 2019, *PASP*, 131, 018002
- Bloemen S. et al., 2011, *MNRAS*, 410, 1787
- Bono G., Marconi M., Stellingwerf R. F., 2000, *A&A*, 360, 245
- Burdge K. et al., 2020a, *ApJ*, 905, 32
- Burdge K. et al., 2020b, *ApJ*, 905, L7
- Butler K., Giddings J. R., 1985, Newsletter of Analysis of Astronomical Spectra, 9. Univ. London, London
- Byrne C. M., Jeffery C. S., 2018, *MNRAS*, 481, 3810
- Byrne C. M., Jeffery C. S., 2020, *MNRAS*, 492, 232
- Byrne C. M., Stanway E. R., Eldridge J. J., 2021, *MNRAS*, 507, 621
- Chambers K. C. et al., 2016, preprint ([arXiv:1612.05560](https://arxiv.org/abs/1612.05560))
- Coppejans R. et al., 2013, *PASP*, 125, 976
- Copperwheat C. M. et al., 2011, *MNRAS*, 410, 1113
- Corradi R. L. M., Schwarz H. E., 1995, *A&A*, 293, 871
- Drake A. J. et al., 2013, *AJ*, 763, 32
- Drew J. E. et al., 2014, *MNRAS*, 440, 2036
- Eldridge J. J., Stanway E. R., Xiao L., McClelland L. A. S., Taylor G., Ng M., Greis S. M. L., Bray J. C., 2017, *Publ. Astron. Soc. Aust.*, 34, e058
- Foreman-Mackey D., Hogg D. W., Lang D., Goodman J., 2013, *PASP*, 125, 306
- Luri X. et al., 2018, *A&A*, 616, A9
- Gaia Collaboration et al., 2021, *A&A*, 649, A1
- Gastine T., Dintrans B., 2008, *A&A*, 490, 743
- Gianninas A., Strickland B. D., Kilic M., Bergeron P., 2013, *ApJ*, 766, 3
- Giddings J. R., 1981, PhD thesis, University of London
- Graham M. J. et al., 2019, *PASP*, 131, 078001
- Green G. M. et al., 2018, *MNRAS*, 478, 651
- Green G. M., Schlafly E., Zucker C., Speagle J. S., Finkbeiner D., 2019, *ApJ*, 887, 93
- Hartman J. D., Gaudi B. S., Holman M. J., McLeod B. A., Stanek K. Z., Barranco J. A., Pinsonneault M. H., Kalirai J. S., 2008, *ApJ*, 675, 1254
- Heber U., 2016, *PASP*, 128, h2001
- Hertzsprung E., 1926, *Bull. Astron. Inst. Neth.*, 3, 115
- Hutchens Z. L., Barlow B. N., Vasquez Soto A., Reichart D. E., Haislip J. B., Kouprianov V. V., Linder T. R., Moore J. P., 2017, *Open Astron.*, 26, 252
- Irrgang A., Kreuzer S., Heber U., Brown W., 2018, *A&A*, 615, L5
- Kepler S. O. et al., 2016, *MNRAS*, 455, 3413
- Kilkenny D., 2010, *Ap&SS*, 329, 175
- Kilkenny D., Koen C., O'Donoghue D., Stobie R. S., 1997, *MNRAS*, 285, 640
- Kobulnicky H. A., Nordsieck K. H., Burgh E. B., Smith M. P., Percival J. W., Williams T. B., O'Donoghue D., 2003, in Iye M., Moorwood A. F. M., eds, Proc. SPIE Conf. Ser. Vol. 4841, Instrument Design and Performance for Optical/Infrared Ground-based Telescopes. SPIE, Bellingham, p. 1634
- Koen C., O'Donoghue D., Kilkenny D., Lynas-Gray A. E., Marang F., van Wyk F., 1998, *MNRAS*, 296, 317
- Kruckow M. U., Neunteufel P. G., Di Stefano R., Gao Y., Kobayashi C., 2021, *ApJ*, 920, 86
- Kupfer T. et al., 2019, *ApJ*, 878, L35
- Kupfer T. et al., 2020, *ApJ*, 898, L25
- Kupfer T. et al., 2021, *MNRAS*, 505, 1254
- Kupfer T. et al., 2022, *ApJ*, 925, L12
- Kurucz R., 1996, ASP Conf. Ser., 108, 160
- Loeb A., Gaudi B. S., 2003, *ApJ*, 588, L117
- Lynas-Gray A. E., 2021, *Frontiers Astron. Space Sci.*, 8, 19
- Macfarlane S. A., Toma R., Ramsay G., Groot P. J., Woudt P. A., Drew J. E., Barentsen G., Eislöffel J., 2015, *MNRAS*, 454, 507
- Macfarlane S. A. et al., 2017a, *MNRAS*, 465, 434
- Macfarlane S. A. et al., 2017b, *MNRAS*, 470, 732
- McWhirter P. R., Lam M. C., 2022, *MNRAS*, 511, 4971
- Mihalas D., 2003, in Hubeny I., Mihalas D., Werner K., eds, ASP Conf. Ser. Vol. 288, Stellar Atmosphere Modeling. Astron. Soc. Pac., San Francisco, p. 471
- Napiwotzki R., Karl C. A., Lisker T., Heber U., Christlieb N., Reimers D., Nelemans G., Homeier D., 2004, *Astrophys. Space Sci.*, 291, 321
- Naslim N., Jeffery C. S., Hibbert A., Behara N. T., 2013, *MNRAS*, 434, 1920
- Pelisolì I., Kepler S. O., Koester D., Romero A. D., 2016, in Tremblay P. E., Gänsicke B., Marsh T., eds, ASP Conf. Ser. Vol. 509, 20th European White Dwarf Workshop. Astron. Soc. Pac. San Francisco, p. 447
- Pietrukowicz P., Latour M., Angeloni R., di Mille F., Soszyński I., Udalski A., Germanà C., 2015, *Acta Astron.*, 65, 63
- Pietrukowicz P. et al., 2017, *Nature Astron.*, 1, 166
- Plachy E. et al., 2021, *ApJS*, 253, 11
- Press W. H., Teukolsky S. A., Vetterling W. T., Flannery B. P., 1992, Numerical recipes in FORTRAN. The Art of Scientific Computing, 2nd edn. Cambridge Univ. Press, New York
- Przybilla N., Nieva M.-F., Butler K., 2011, *JPhCS*, 328a2015P
- Ramsay G., 2018, *A&A*, 620, L9
- Reed M. et al., 2004, *MNRAS*, 348, 1164
- Romero A. D., Córscico A. H., Althaus L. G., Pelisolì I., Kepler S. O., 2018, *MNRAS*, 477, L30
- Schaffenroth V. et al., 2021, *MNRAS*, 501, 3847
- Shappee B. J. et al., 2014, *ApJ*, 788, 48
- Taylor M. B., 2006, in Gabriel C. ed., ASP Conf. Ser. Vol. 351, Astronomical Data Analysis Software and Systems XV. Astron. Soc. Pac., San Francisco, p. 666
- Toma R. et al., 2016, *MNRAS*, 463, 1099
- Udalski A., Szymański M. K., Szymański G., 2015, *Acta Astron.*, 65, 1
- Vennes S., Kawka A., O'Toole S. J., Németh P., Burton D., 2012, *ApJ*, 759, L25
- Verbunt F., Rappaport S., 1988, *ApJ*, 332, 193
- Wozniak P. R., 2000, *Acta Astron.*, 50, 421
- Zechmeister M., Kürster M., 2009, *A&A*, 496, 577

This paper has been typeset from a $\text{\TeX}/\text{\LaTeX}$ file prepared by the author.